Research Article

NEURAL REGENERATION RESEARCH
www.nrronline.org

Sox2-overexpressing neural stem cells alleviate ventricular enlargement and neurological dysfunction in posthemorrhagic hydrocephalus

Baocheng Gao[1, 2, #], Haoxiang Wang[1, #], Shuang Hu[3, #], Kunhong Zhong[1], Xiaoyin Liu[1], Ziang Deng[1], Yuanyou Li[1], Aiping Tong[4, *], Liangxue Zhou[1, 5, 6, *]

https://doi.org/10.4103/NRR.NRR-D-24-01491

Date of submission: November 29, 2024

Date of decision: February 19, 2025

Date of acceptance: March 17, 2025

Date of web publication: April 30, 2025

From the Contents

Graphical Abstract

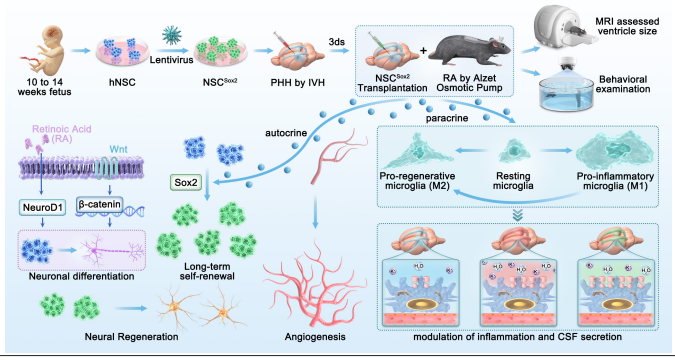

Abstract

Neural stem cells (NSCs) have the potential for self-renewal and multidirectional differentiation, and their transplantation has achieved good efficacy in a variety of diseases. However, only 1%–10% of transplanted NSCs survive in the ischemic and hypoxic microenvironment of posthemorrhagic hydrocephalus. Sox2 is an important factor for NSCs to maintain proliferation. Therefore, Sox2-overexpressing NSCs (NSC^{Sox2}) may be more successful in improving neurological dysfunction after posthemorrhagic hydrocephalus. In this study, human NSC^{Sox2} was transplanted into a posthemorrhagic hydrocephalus mouse model, and retinoic acid was administered to further promote NSC differentiation. The results showed that NSC^{Sox2} attenuated the ventricular enlargement caused by posthemorrhagic hydrocephalus and improved neurological function. NSC^{Sox2} also promoted nerve regeneration, inhibited neuroinflammation and promoted M2 polarization (anti-inflammatory phenotype), thereby reducing cerebrospinal fluid secretion in choroid plexus. These findings suggest that NSC^{Sox2} rescued ventricular enlargement and neurological dysfunction induced by posthemorrhagic hydrocephalus through neural regeneration and modulation of inflammation.

Key Words: angiogenesis; cerebrospinal fluid; hippocampal transplantation; inflammation; microglia; neural stem cells; neurogenesis; posthemorrhagic hydrocephalus; retinoic acid; Sox2

Introduction

Posthemorrhagic hydrocephalus (PHH) often occurs after germinal matrix hemorrhage in preterm infants with low body weight (< 1500 g) and intraventricular hemorrhage (IVH) in adults (Garcia-Bonilla et al., 2022). It is characterized by enlarged ventricles, which cause increased intracranial pressure, ischemic-hypoxic damage, axonal breakage, synaptic loss, microglial activation and astrocytic hyperplasia (Garcia-Bonilla et al., 2022), resulting in severe cognitive and motor impairments. Currently, the main treatment modalities are a cerebrospinal fluid (CSF) shunt or endoscopic ventriculostomy, which can resolve symptoms in the short term. Yet, some studies have reported that more than 50% of patients within 2 years and more than 70% of patients within 10 years of operation undergo shunt failure and need multiple surgical operations (Karimy et al., 2020; Dong et al., 2024). Furthermore, endoscopic ventriculostomy requires more advanced surgical techniques and carries high perioperative risks, and there are still many unknowns regarding its long-term outcomes (Jeong and Jurisch-Yaksi, 2023). Importantly, even if the ventricle size decreases after surgery, the neurological deficits that have already occurred in some patients are often difficult to completely reverse (Hersh et al., 2021). Thus, there is an urgent need to find new therapeutic strategies to provide better treatment options for patients with PHH.

Neural stem cell (NSC) transplantation has been considered the most

[1]Department of Neurosurgery, West China Medical School, West China Hospital, Sichuan University, Chengdu, Sichuan Province, China; [2]Department of Neurosurgery, The First People's Hospital of Yunnan Province, The Affiliated Hospital of Kunming University of Science and Technology, Kunming, Yunnan Province, China; [3]Department of Otolaryngology & Head and Neck Surgery, The First People's Hospital of Yunnan Province, The Affiliated Hospital of Kunming University of Science and Technology, Kunming, Yunnan Province, China; [4]State Key Laboratory of Biotherapy and Cancer Center, Research Unit of Gene and Immunotherapy, Chinese Academy of Medical Sciences, Collaborative Innovation Center of Biotherapy, West China Hospital, Chengdu, Sichuan Province, China; [5]Department of Neurosurgery, NHC Key Laboratory of Nuclear Technology Medical Transformation (Mianyang Central Hospital),School of Medicine, University of Electronic Science and Technology of China, Mianyang, Sichuan Province, China; [6]Department of Neurosurgery, Fifth People's Hospital of Ningxia Hui Autonomous Region, Shizuishan, Ningxia Hui Autonomous Region, China

*Correspondence to: Liangxue Zhou, MD, PhD, zhlxlll@163.com; Aiping Tong, MD, PhD, aipingtong@scu.edu.cn.

https://orcid.org/0000-0001-9991-6358 (Liangxue Zhou); https://orcid.org/0000-0002-3392-5443 (Aiping Tong)

#These authors contributed equally to this work and share first authorship.

Funding: *This study was supported by the National Natural Science Foundation of China, Nos. 82473334 (to LZ), 82401629 (to XL); the Major Scientific and Technological Achievements Transformation Project of Ningxia Hui Autonomous Region, No. 2022CJE09013 (to LZ); Mianyang Science and Technology Bureau (Mianyang Science and Technology Program), No. 2023ZYDF097 (to LZ); NHC Key Laboratory of Nuclear Technology Medical Transformation (Mianyang Central Hospital), No. 2023HYX001 (to LZ); Spinal Cord Diseases Clinical Medical Center of Yunnan Province, No. 2024JSKFKT-16 (to BG); the Natural Science Foundation of Sichuan Province, No. 2024NSFSC1646 (to XL); and the China Postdoctoral Science Foundation, Nos. GZC20231811 (to XL), 2024T170601 (to XL) and 2024M76228 (to XL).*

How to cite this article: *Gao B, Wang H, Hu S, Zhong K, Liu X, Deng Z, Li Y, Tong A, Zhou L (2026) Sox2-overexpressing neural stem cells alleviate ventricular enlargement and neurological dysfunction in posthemorrhagic hydrocephalus. Neural Regen Res 21(2):769-779.*

promising therapeutic measure for the treatment of neurological disorders such as Parkinson's disease, motor neuron disease, and hemorrhagic cerebrovascular diseases (Temple, 2023; Sheikh et al., 2024). This is because NSCs can differentiate into neurons and integrate into the existing synaptic network to replace damaged or lost neurons (Zhang et al., 2019; Ji et al., 2023). Additionally, NSCs can play a paracrine role by releasing nutritional and immunomodulatory factors that regulate many pathogenic pathways involved in the development of PHH (Garcia-Bonilla et al., 2022). Recent studies have demonstrated that human NSC (hNSC) transplantation significantly improves motor and cognitive functions in murine models of Parkinson's and Huntington's diseases, and have also shown that hNSCs differentiate into neurons, glial cells and oligodendrocytes in model mice (Park et al., 2021; Baloh et al., 2022). However, after PHH, transplanted NSCs do not survive and reproduce in the microenvironment of ischemia and hypoxia; a previous study showed that only 1%–10% of transplanted NSCs survive (Wang et al., 2024). Therefore, transplantation of gene-edited NSCs that promote NSC proliferation and differentiation may be more effective for slowing disease progression, enhancing cell function, or controlling cell states in specific disease conditions (Temple, 2023; Wang et al., 2024).

Sex-determining region Y-box 2 (Sox2), as an important stem cell transcription factor, maintains NSC self-renewal, promotes nervous system development and maintains NSC numbers *in vivo* through a Sox2-dependent autocrine mechanism. A previous study showed that Sox2 deficiency led to impaired hippocampal neural regeneration and a reduced number of NSCs (Pagin et al., 2021). Retinoic acid (RA) is a metabolite of vitamin A that promotes the differentiation of NSCs into neurons (Kubickova et al., 2023). Therefore, it is reasonable to believe that transplantation of hNSCs transfected with Sox2 and concomitant administration of RA would better promote the functional and structural repair of PHH through three mechanisms. First, the self-renewal and differentiation ability of NSCs would be enhanced to more effectively differentiate into mature effector cells to replace damaged cells. Second, the paracrine mechanism of NSCs would provide neuroprotection (Rajendran et al., 2025). Third, the local microenvironment would be regulated by modulating inflammation (Zhang et al., 2023).

In this study, human embryonic NSCs transfected with Sox2 were transplanted into the hippocampus of a PHH C57BL/6j mouse model. We investigated the effect and safety of this application by observing the behavioral changes of the model mice before and after the transplantation, and by detecting the changes in their neural regeneration and inflammatory factors. The findings will help provide a theoretical basis for the clinical treatment of PHH. Furthermore, we have compiled the most recent advances in NSC engineering and presented viable techniques for enhancing hNSC survival and treatment efficiency in the harsh microenvironment of PHH.

Methods

Animals

To conduct our experimental procedures, 6- to 8-week-old C57BL/6j male mice (weighing 18–24 g) were used, and all experimental procedures were approved by the Experimental Animal Ethics Committee of West China Hospital (Approval No. 20230426002). The C57BL/6j strain was sourced from the Laboratory Animal Center of Sichuan University (Chengdu, Sichuan Province). The animals were maintained in a specific pathogen-free environment with controlled temperature (20°C to 26°C) and humidity (40% to 60%), a 12-hour light/dark cycle, and *ad libitum* access to food and water. Given the reported anti-neuroinflammatory effects of estrogen, female mice were excluded from the study to prevent potential confounding influences of steroid hormones. All animal experiments adhered to the National Institutes of Health guidelines for the Care and Use of Laboratory Animals (National Research Council, 2011) and were approved by the Animal Care and Use Committee of Sichuan University (approval No. 20230426002) on April 26, 2023.

The mice were randomly divided into a sham group, IVH group (PHH group), sham transplantation group (PBS group), NSC group, and experimental group (NSC^{Sox2} group) using a blinded allocation method. The weight changes of each group were recorded daily.

Mouse model of intraventricular hemorrhage

The IVH model was established using a previously published method (Cao et al., 2023). Specifically, mice were anesthetized via intraperitoneal injection of pentobarbital (40 mg/kg; Sigma, St. Louis, MO, USA) and secured in a stereotaxic apparatus (RWD Life Science Co., LTD, Shenzhen, Guangdong, China). The dorsal aspect of the skull was shaved, and the skin was incised along the midline of the neck using a new surgical blade. Under sterile conditions, the skin was retracted bilaterally using Barraquer retractors (Harvard Apparatus, Hopkinton, MA, USA) to expose the underlying muscles and the top of the skull. The skull surface was cleaned with a 0.9% saline solution and dried with sterile gauze sponges (Covidien, Mansfield, MA, USA). The periosteum was etched with hydrogen peroxide to reveal the fontanelle. Once the skull was dry, a high-speed drill was used to create a 1-mm burr hole (coordinates relative to bregma: x = 1.0 mm, y = –0.5 mm) above the right lateral ventricle. A sterile 1-mL microinjector was used to collect approximately 40 µL of autologous blood from the tail vein of each mouse, which was then transferred to a 100 µL syringe (Hamilton, Reno, NV, USA) and injected into the right ventricle through the burr hole (Cao et al., 2023) (coordinates relative to bregma: z = –2.5 mm) at a rate of 5 µL/min. Following the injection, the needle was left in place for 20 minutes before being slowly withdrawn at a rate of 0.5 mm/min. The incision was closed using absorbable surgical sutures with a simple continuous stitch. Mice in the sham surgery group underwent scalp incision, skull perforation and needle insertion.

Primary extraction of neural stem cells

NSCs were obtained from the telencephalon of a 10- to 12-week postconception human fetus, after elective pregnancy termination. The use of hNSCs was approved by the Medical Ethics Committee of West China Hospital (Chengdu, Sichuan Province, China; approval No. 2023-527; June 20, 2023), and their use for therapeutic application adheres to medical ethics. For hNSC collection, the fetal brain cortex was peeled off under aseptic conditions, and the surface blood vessels were removed and then rinsed three times with phosphate buffer saline (PBS). In culture medium containing Dulbecco's modified Eagle medium/nutrient mixture F-12 (Wandao Biotechnology Development Co., Ltd., Chengdu, China), the fetal brain cortex was fully sheared with ophthalmic scissors, and then digested with Accutase (Cat# A1110501, Gibco, Waltham, MA, USA) for approximately 5 minutes. The tissue was then washed with PBS three times, followed by pipetting to break up the cell mass. The cell suspension was transferred into a centrifuge tube and centrifuged at 1000 r/min for 5 minutes. The supernatant was removed and filtered with a 70-mesh filter. NSCs were cultured in a serum-free medium supplemented with epidermal growth factor (20 ng/mL, Peprotech, Andover, NJ, USA), basic fibroblast growth factor (10 ng/mL, Peprotech), and B27 (10%, Gibco) on vessels coated with laminin (20 µg/mL, Sigma) in an incubator at 37°C and humidified atmosphere containing 5% CO_2. Neurospheres approximately 150 µm in diameter were formed by incubation for 3–4 days, and the solution was aspirated with a micropipette and passed through 100-µm and 40-µm filters for mechanical dispersion. Immunofluorescence staining showed that nestin and Sox2 were highly expressed in the neurospheres. After two passages, the cells were used for the experiments. For differentiation, culture vessels were coated with a thin layer of Matrigel™ (1:30 dilution) in plain Dulbecco's modified Eagle medium for 18 hours at 4°C, followed by 30 minutes at 37°C. The coating solution was then replaced with prewarmed differentiation medium (Dulbecco's modified Eagle medium/nutrient mixture F-12 + 20% fetal bovine serum) before cell seeding. To test its effects on NSC differentiation, RA (1 µm/µL, Wandao Biotechnology Development Co., LTD) was added to the differentiation medium every 4 days, for a total of eight times.

Lentivirus transfection

Construction of the GFP-expressing lentivirus, Sox2-expressing lentivirus, GFP + Sox2-expressing lentivirus and luciferase + Sox2-expressing lentivirus was previously described (Favaro et al., 2009). The NSC spheres were mechanically dispersed and digested with Accutase into single cells, which were then inoculated into 6-well plates at 2×10^6 cells/well. The cells were transduced at multiplicities of infection of 10 overnight. The following day, the medium was changed to serum-free NSC medium (Wandao Biotechnology Development Co., LTD). Lentivirus-transfected NSC^{Sox2} cells, $NSC^{GFP+Sox2}$ cells and $NSC^{luciferase+Sox2}$ cells were prepared.

Cell transplantation

All mice were injected intraperitoneally with cyclosporine A (10 mg/kg, Wandao Biotechnology Development Co., LTD) 2 days before surgery and 5 mg/kg daily after surgery until execution. We transplanted 5 µL cells (1 ×

10^5) into the NSC and NSC^{Sox2} mice. The grafting procedure was similar to that of the PHH model construction, except that a 25-μL syringe (Hamilton, Reno, NV, USA) containing 5 μL of PBS or cell suspension was used. Cells were transplanted into the right hippocampus (coordinates relative to bregma: x = 2.5 mm, y = –2.0 mm, z = –2.2 mm). Following the injection, the needle was left in place for 10 minutes before being slowly withdrawn at a rate of 0.5 mm/min. Then, the original graft puncture site was inserted with an Alzet Osmotic Pump (Model 813280PPKXXC+1004+1004 Adaptive Transfer Nuclear Magnetic Resonance Pipeline, RWD Life Science Co., Ltd) containing a total of 11 μmol RA. The slow-release capsule pump had a delivery rate of 0.11 μL/h, which was equivalent to an infusion of 8.13 μM of RA for 28 days, and was buried under the dorsal subcutis and secured with dental cement. After drying the cement, the incision was closed using absorbable surgical sutures with a simple continuous stitch.

Luciferase reporter assay

Longitudinal *in vivo* imaging results following the $NSC^{Luciferase+Sox2}$ transplantation were performed at 3, 7, 14, 21, and 28 days. Luciferase fluorescence intensity was analyzed using the Steady-Glo Luciferase assay system (E2520, Promega, Madison, WI, USA) according to the manufacturer's protocol.

Magnetic resonance imaging

Mice were anesthetized using a 2% isoflurane–air mixture (Wandao Biotechnology Development Co., Ltd) during magnetic resonance imaging (MRI). MRI was conducted using a 7.0-Tesla MR scanner (Bruker BioSpec 70/30 MRI, Billerica, MA, USA). A total of 18 coronal slices covering the entire brain were acquired with the following parameters: T2 fast spin-echo sequence, repetition time 4000 ms, echo time 60 ms, field of view 35 × 35 mm^2, matrix 256 × 256, slice thickness 0.5 mm, echo time 2.5 ms and repetition time 100 ms. We used the software Slicer (version 5.6.1, https://slicer.org) to perform the three-dimensional reconstructions (Fedorov et al., 2012; Gonzalo Domínguez et al., 2016). After we segmented the target structure, we used the Model Maker module to generate a surface volume. The bilateral ventricles were outlined, and the ventricular volume was determined.

Open field test

The open field test was conducted to investigate the neuropsychiatric changes in sham group and IVH group at 31 days post-operation, and in PBS, NSC and NSC^{Sox2} groups at 28 days after transplantation (Wei et al., 2021). Specifically, a square open-field arena (100 × 100 cm^2) with black inner walls and a white floor was prepared. The floor was artificially divided into nine grid sections by the computer system. A digital camera tracking system (Pine Technology, Inc., San Mateo County, CA, USA) was installed above the arena to monitor the movement trajectories of the mice. Mice were acclimated to the experimental environment before testing. During the experiment, each mouse was placed at the center of the arena. Each trial lasted for 5 minutes, during which the movements, total duration of active behavior and time spent in the central area were recorded. After each trial, the mice were removed from the arena, and the inner walls and floor were thoroughly cleaned to eliminate any residual cues, such as urine, feces, or odors, thereby preventing contamination of subsequent trials.

Morris water maze test

The Morris water maze test was performed in sham and IVH groups at 31 days post-operation, and in PBS, NSC and NSC^{Sox2} groups at 28 days after transplantation using previously published experimental procedures (Vorhees and Williams, 2006). Mice were placed in a metal pool (50 cm deep and 200 cm in diameter) filled with water that was made opaque using titanium dioxide powder. The pool was divided into four quadrants, and a submerged platform (1–1.5 cm below the water surface, 6 × 6 cm^2) was positioned in the target quadrant. Mice were trained to locate the submerged platform within 60 seconds. They then underwent 5 days of acquisition training using a random set of starting points within the four quadrants. Latency times were recorded and averaged daily. On day 6, the submerged platform was removed and the animals completed a 60-second probe trial. The number of platform crossings, distance traveled and time spent in the target quadrant were measured.

Tissue preparation and biopsy

Mice were anesthetized via intraperitoneal injection of pentobarbital (40 mg/kg) and euthanized by cervical dislocation. The brains were harvested and fixed in 4% paraformaldehyde for 24 hours at room temperature. The brain tissues were then embedded in paraffin and sectioned into 4-μm slices. Images of the tissue slices were directly captured under natural light for histopathological biopsy examination.

Western blot analysis

Protein was extracted from mouse hippocampus, choroid plexus and cultured neurospheres or adherent differentiated cells. The total protein concentration of the supernatant was measured using a bicinchoninic acid protein assay kit (Thermo Fisher Scientific, Waltham, MA, USA). Protein samples were heated at 95°C for 10 minutes. Equal amounts of protein (30 μg, the sample volume was adjusted based on the measured protein concentration) were separated by 8%–12% sodium dodecyl sulfate polyacrylamide gel electrophoresis and transferred to 0.45-μm polyvinylidene fluoride membranes. The membranes were blocked with 5% skim milk, washed twice with Tris-buffered saline with Tween 20 (5 minutes per wash), and then incubated with primary antibodies. The membranes were washed four times (5 minutes per wash) with Tris-buffered saline with Tween 20 and then incubated with horseradish peroxidase-conjugated secondary antibody. The information on antibodies used in this study and corresponding experimental conditions are listed in **Additional Table 1**. Immunoreactive bands were detected using enhanced chemiluminescence. Finally, the optical density ratio of the target protein to glyceraldehyde-3-phosphate dehydrogenase (GAPDH) was calculated using ImageJ software (version 7.4, National Institutes of Health, Bethesda, MD, USA) (Schneider et al., 2012).

Immunofluorescence staining

For immunofluorescence, the 4-μm paraffin sections were initially deparaffinized by incubating the slides in xylene for 10 minutes (twice), 100% ethanol for 5 minutes (twice), 95% ethanol for 5 minutes (twice) and 70% ethanol for 5 minutes (once). Following this, the sections were washed for 5 minutes in distilled water, subjected to antigen retrieval using citrate-based buffer (Retrieve-all system 1, Biolegend, San Diego, CA, USA) at 95°C for 30 minutes, then washed again three times with PBS with Tween 20. Separately, cells were washed three times in PBS and then fixed in 4% paraformaldehyde for 15 minutes at room temperature. Next, the cells were permeabilized with 0.3% Triton X-100 for 15 minutes. Both the cells and brain sections were incubated in blocking solution (10% goat serum in PBS with Tween 20) for 1 hour at room temperature. The information on antibodies used in this study and corresponding experimental conditions are listed in **Additional Table 1**. After three washes with PBS with Tween 20, secondary antibodies and 4′,6-diamidino-2-phenylindole (5 μg/mL, Biolegend) were applied to the sections, which were then incubated for 2 hours at room temperature. Finally, the sections were treated with an anti-fluorescence quencher sealer (Servicebio, Wuhan, Hubei, China), and images were captured within 8 hours using fluorescence microscopy (Zeiss, Jena, Germany). A researcher blinded to experimental groups examined the stained slides under a fluorescence microscope and randomly selected four positions at a 20× or 40× field of view to capture images. The average percentage of positive cells was analyzed using ImageJ software.

Flow cytometry

To perform flow cytometry analysis, cultured neurospheres were collected and digested into single cells by mechanical dispersion and Accutase enzyme. The cells were centrifuged and fixed with 4% paraformaldehyde for 30 minutes. After fixation, the cells were collected by centrifugation and washed twice with PBS to remove excess fixative. Next, the cells were resuspended in PBS containing 0.1% saponin permeabilization buffer and incubated on ice for 10 minutes to facilitate membrane permeabilization. Subsequently, the cells were washed twice with PBS and resuspended in PBS containing 1% bovine serum albumin to reduce nonspecific binding, and then incubated with directly labeled antibodies in the dark. Following incubation, the cells were washed three times with PBS and analyzed using a flow cytometer (BD Biosciences, San Jose, CA, USA). Data processing and analysis were performed using FlowJo software (Tree Star, Ashland, OR, USA).

Enzyme-linked immunosorbent assay

A hippocampal tissue block was excised and washed in precooled PBS to remove the blood. The tissue block was then transferred into a glass homogenizer and 0.9% saline was added at the ratio of weight (mg): volume

(μL) = 1:9 in an ice-water bath. The tissue was mechanically homogenized and prepared as 10% homogenate, then centrifuged at 2500 × *g* for 10 minutes. The supernatant was collected for the assay using enzyme-linked immunosorbent assay (ELISA) kits (EK0527, EK0394, Boster Bio, Anaheim, CA, USA). The procedures were performed according to a previously published method (Wang and Zhang, 2022).

Statistical analysis

The data analyses were performed by independent researchers who did not participate in the design or execution of the experiments. Before the study began, an analysis was conducted to determine that a minimum sample size of $n = 5$ for behavioral assessment and $n = 3$ for biochemical analysis would provide sufficient statistical power with $\alpha = 0.05$ (two-tailed). Statistical data were analyzed using one-way or two-way analysis of variance, followed by *post hoc* Tukey's honestly significant difference test to compare differences between three or more groups using GraphPad Prism (version 10.0.0 for Windows, GraphPad Software, Boston, MA, USA, www.graphpad.com). Differences between two experimental groups were assessed using Student's *t*-test. All data are presented as the mean ± standard deviation. A *P*-value < 0.05 was considered statistically significant.

Results

Construction and transplantation of NSC^{Sox2}

To investigate our hypothesis, we first extracted embryonic stem cells from human embryonic brains for cultivation. After extracting the stem cells, we propagated NSCs and transduced Sox2 using lentiviruses to increase Sox2 expression in the NSCs. Double immunofluorescence staining for nestin and Sox2 showed that the lentivirus-transduced NSCs had higher Sox2 fluorescence intensity, quantitative analysis of the mean fluorescent intensity of Sox2 before and after transfection was 48.30 ± 3.51 and 66.39 ± 5.49, respectively ($P < 0.05$; **Figure 1A** and **B**). We also extracted proteins from the NSCs and performed western blot analysis, the Sox2 expression normalized to GAPDH demonstrated a 1.6-fold elevation from 0.79 ± 0.08 (pre-transduction) to 1.29 ± 0.06 (post-transduction) ($P < 0.05$; **Figure 1C** and **D**). Additionally, immunofluorescence assay using a GFP reporter gene also confirmed the successful construction of NSC^{Sox2} cells using lentivirus (**Figures 1E**). Research has shown that RA plays a crucial role in NSC differentiation during development (Pagin et al., 2021). Here, we used flow cytometry to analyze neuronal differentiation in the different groups,which showed NeuN$^+$ cells in NSC, NSC^{Sox2} and NSC^{Sox2} with RA groups were 33.11%, 50.90% and 57.91%, respectively (**Figure 1F** and **G**). The results showed that Sox2 promoted the proliferation of NSCs, and RA further enhanced this proliferation. Subsequently, we used double immunofluorescence staining to examine the differentiation of NSCs into neural progenitor cells (DCX$^+$) and neurons (NeuN$^+$). After adding RA, the number of DCX$^+$ cells decreased significantly, whereas the number of NeuN$^+$ cells increased from 18.46% to 37.04% (**Figure 1H** and **I**).

Subsequently, we used a brain microinjection pump to inject the NSC$^{Sox2+GFP}$ or NSC$^{Sox2+luciferase}$ into the hippocampus of PHH mice (**Figure 2A**). **Figure 2B** shows that the transplanted NSC$^{Sox2+GFP}$ cells were all located in the hippocampus, even with enlarged ventricles after PHH. After the transplantation, we closely monitored the distribution of the transplanted NSC$^{Sox2+luciferase}$ cells using an *in vivo* imaging system at various time points. Our results showed that starting at 14 days after transplantation, the NSCs rapidly proliferated and gradually spread throughout the whole brain at subsequent time points (**Figure 2C**).

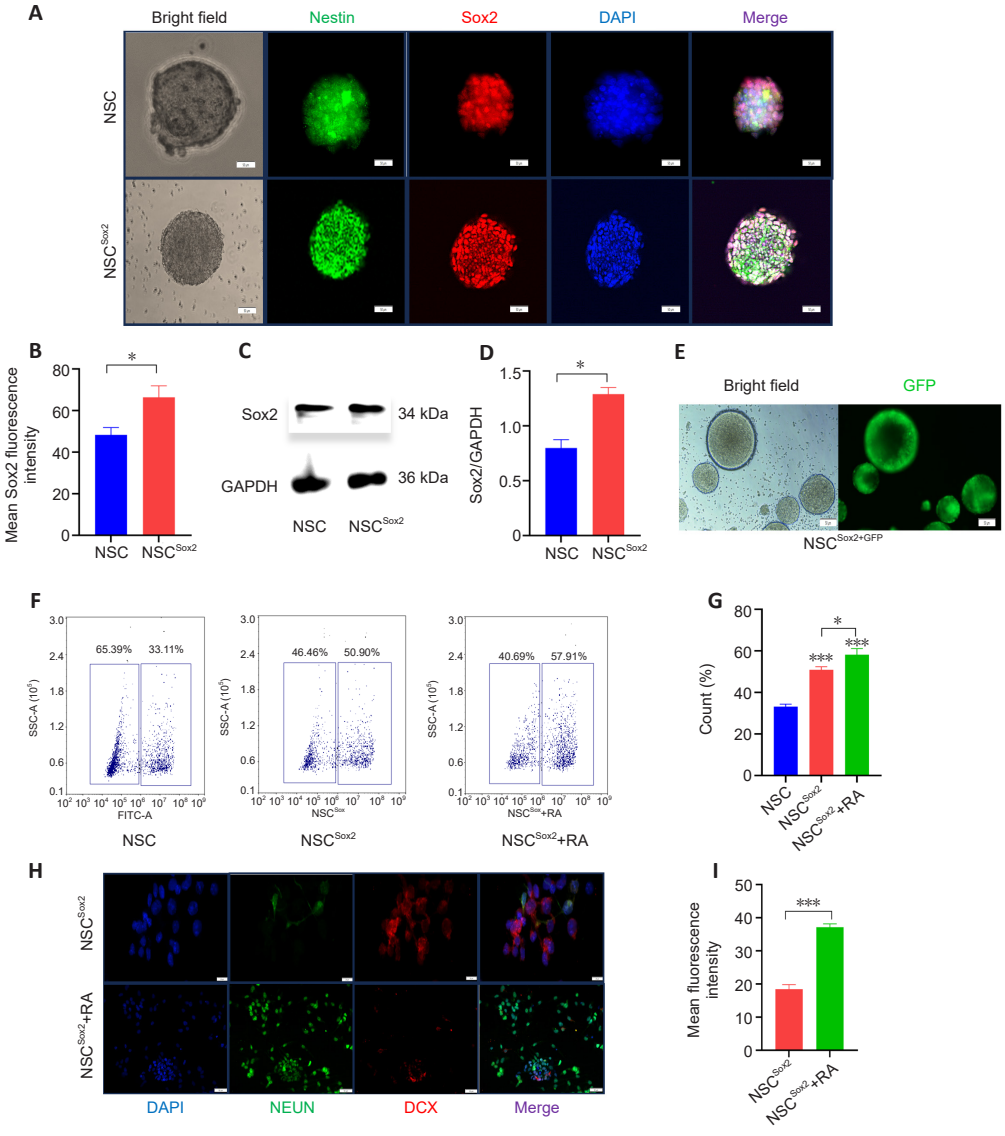

Figure 1 | Transfection and differentiation of NSC^{Sox2}.
(A) Representative images of nestin (green, fluorescein isothiocyanate) and Sox2 (red, rhodamine) immunoreactivity in NSCs before and after transfection, observed by fluorescence microscopy. Scale bars: 50 μm. (B) Mean fluorescence intensity of Sox2. (C) Representative bands of Sox2 expression in NSCs before and after transfection. (D) Quantitative analysis of Sox2 protein expression. (E) Representative images of NSCs transfected with Sox2 + GFP, observed by fluorescence microscopy. Scale bars: 50 μm. (F) Flow cytometry analysis of the proportion of NeuN$^+$ cells. (G) Flow cytometry of NeuN$^+$ cells. (H) Representative images of NeuN (green, CoraLite488) and DCX (red, Cyanine-3) expression in different groups, observed by fluorescence microscopy. Scale bars: NSC^{Sox2}, 20 μm; NSC^{Sox2}+RA, 50 μm. (I) Mean fluorescence intensity of NeuN$^+$ cells. All data are presented as the mean ± SD ($n = 3$). *$P < 0.05$, ***$P < 0.001$ (Student's *t*-test). DAPI: 4′,6-Diamidino-2-phenylindole; DCX: doublecortin; GAPDH: glyceraldehyde-3-phosphate dehydrogenase; GFP: green fluorescent protein; NeuN: neuron-specific nuclear protein; NSCs: neural stem cells; RA: retinoic acid; Sox2: sex-determining region Y-box 2.

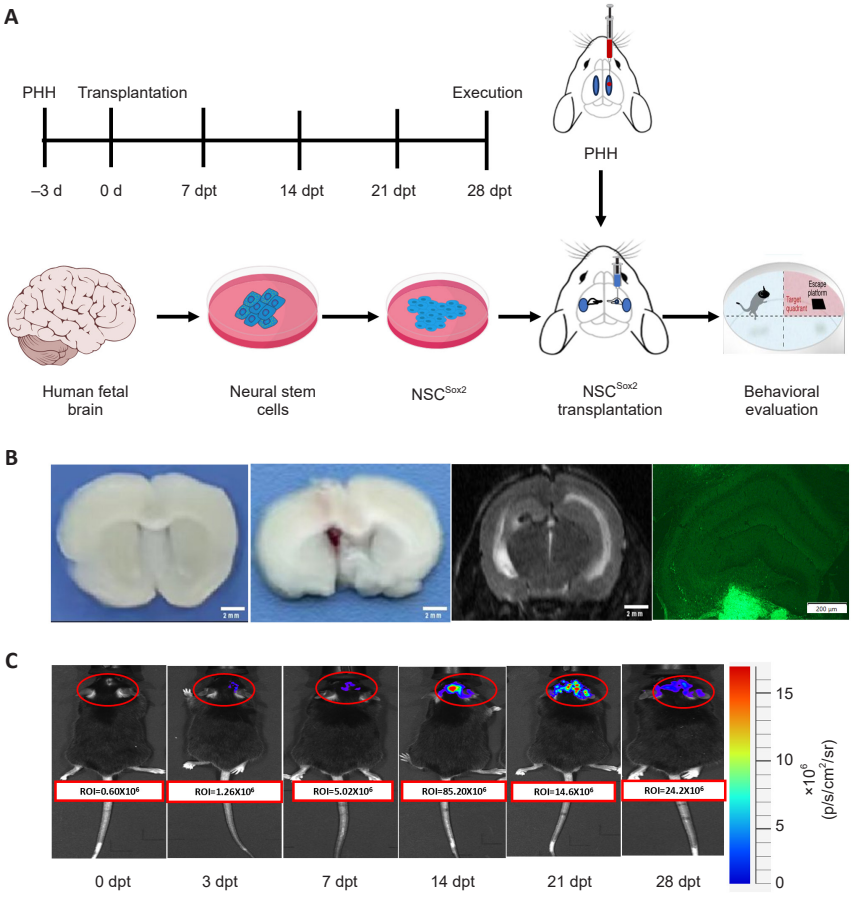

Figure 2 | Human NSC transplantation into PHH mouse model.

(A) Experiment timeline and illustration of the extraction of human NSCs from embryonic brains, their cultivation and induction to overexpress SOX2, followed by transplantation into a PHH mouse model for behavioral assessment. (B) Coronal section showing PHH model by IVH. The biopsy and MRI images showed that the $NSC^{Sox2+GFP}$ transplantation site was located in the hippocampus. Scale bars: 2 mm and 200 μm, respectively. (C) Longitudinal *in vivo* imaging results following the $NSC^{Sox2+luciferase}$ transplantation. Red circle indicates the region of interest. dpt: Day post-transplamtation; GFP: green fluorescent protein; IVH: intraventricular hemorrhage; MRI: magnetic resonance imaging; NSCs: neural stem cells; PHH: posthemorrhagic hydrocephalus; ROI: region of interest; Sox2: sex-determining region Y-box 2.

NSC^{Sox2} transplantation ameliorates ventricular volume enlargement induced by intraventricular hemorrhage

To investigate the effects of NSC transplantation on mice with PHH, MRI was used to examine the ventricular morphology and measure ventricular size. Quantitative analysis of ventricular volume showed that there was no statistical significance between the 1 day (1.86 ± 0.28 mm^3) and the 31 day (2.62 ± 0.65 mm^3) in sham group. At the same time, it was found that ventricle enlargement appeared significantly in IVH3d group (5.46 ± 1.09 mm^3), while the extent of ventricle enlargement was significantly delayed in the pt-3w group (6.09 ± 1.21 mm^3). The largest increase in ventricle size during the acute phase occurred 3 days after IVH (**Figure 3A** and **B**). Therefore, we chose this time point for NSC^{Sox2} transplantation, which corresponds to the clinical time frame when ventriculoperitoneal shunting is typically required due to high intracranial pressure. Following transplantation, we further monitored the changes in ventricular size via MRI. We found that NSC^{Sox2} transplantation significantly reduced the ventricular size in IVH mice at the same time point (**Figure 3A** and **B**). The effect was not observed in the control group that received PBS injections.

NSC^{Sox2} transplantation ameliorates learning, cognitive, and memory functions in intraventricular hemorrhage mice

To investigate the effects of NSC^{Sox2} transplantation on learning, cognitive, and memory functions in IVH mice, we conducted the open field and Morris water maze tests. In the open field test, IVH mice had reduced total movement distance (9.37 ± 1.95 m) and spent more time in the corners (80.47% ± 4.88%) (**Figure 4A–C**). However, these changes were significantly improved following NSC transplantation. Specifically, NSC^{Sox2} transplantation increased the movement distance of the mice. This suggests that NSC^{Sox2} transplantation helped restore the neurological and motor function deficits and enhanced exploratory behavior in IVH mice. Similarly, in the Morris water maze, IVH mice had a significantly reduced number of platform crossings (0.67 ± 0.52) and spent less time in the target quadrant (24.94% ± 3.08%), suggesting impaired learning and memory functions. However, in NSC group, the number of platform crossings increased significantly, although the time spent in the target quadrant did not change (**Figure 4D–F**). However, in NSC^{Sox2} group, the number of platform crossings and the time spent in the target quadrant were significantly improved.

NSC^{Sox2} transplantation promotes neuronal regeneration, angiogenesis, and M2 polarization of microglia in mice with intraventricular hemorrhage

Next, we investigated the specific mechanisms by which transplanted NSCs improve neurological function in IVH mice. Hippocampal neuronal activity is fundamental to learning and memory formation (Tobin et al., 2019). Therefore, we examined the expression of DCX cells in the hippocampus, which can indirectly reflect neuronal regeneration. The average DCX fluorescence intensity shown by immunofluorescence was 3183.85 ± 210.18 (sham group), 1226.27 ± 92.87 (IVH group), 1755.97 ± 100.35 (NSC group) and 2535.07 ± 183.90 (NSC^{Sox2} group), respectively. Our results showed that after NSC transplantation, the IVH-induced decrease in the number of DCX-positive cells in the hippocampus was improved. This improvement was greater when NSC^{Sox2} were transplanted (**Figure 5A** and **B**).

In addition, we examined the effects of transplanted NSCs on angiogenesis and synaptophysin expression. Compared with sham group (0.99 ± 0.15), the relative fluorescence intensity of CD31 was significantly decreased in the IVH group (0.36 ± 0.40), but not in the Trans NSC^{Sox2} group (0.77 ± 0.07). The relative fluorescence intensity of SYP in sham, IVH and Trans NSC^{Sox2} groups were 1271.67 ± 18.30, 119.83 ± 26.00 and 410.50 ± 20.90, respectively (**Figure 6A–C**). The results showed that IVH downregulated synaptophysin and CD31 expression, and that NSC transplantation increased synaptophysin expression. NSC transplantation did not improve CD31 expression, but NSC^{Sox2} transplantation restored the downregulation of CD31 expression induced by IVH. We also investigated the impact of NSC transplantation on microglia. Double immunofluorescence staining showed the percentages of Iba-1 & iNOS positive cells in sham group, IVH group and NSC^{Sox2} group were 6.77% ± 1.70%, 61.3% ± 5.44% and 14.13% ± 2.83%, respectively, and the percentages of Iba-1 & CD206 positive cells were 14.65% ± 2.26%, 9.08% ± 1.88%, and 32.97% ± 4.20%, respectively. The results showed that NSC transplantation reduced the increase in M1-type microglia (inducible nitric oxide synthase $(iNOS)^+$/ionized calcium-binding adapter molecule 1 $(Iba\text{-}1)^+$) induced by IVH. NSC transplantation did not significantly induce polarization of microglia towards the M2 phenotype ($CD206^+/Iba\text{-}1^+$), whereas NSC^{Sox2} transplantation promoted M2-type polarization of microglia (**Figure 6D–F**).

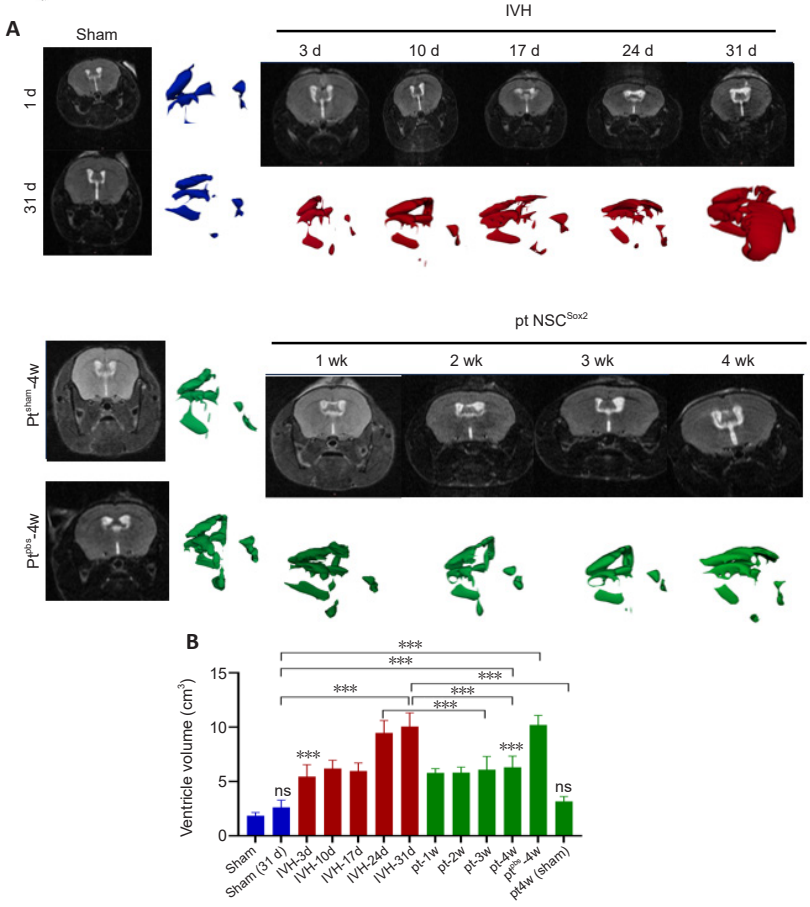

Figure 3 | Morphological changes in the ventricles before and after NSC^{Sox2} transplantation.

(A) Representative images of ventricular morphology at multiple time points after IVH. (B) Quantitative analysis of ventricular volume in different groups. All data are presented as the mean ± SD (n = 5). ***P < 0.001 (one-way analysis of variance followed by *post hoc* Tukey's honestly significant difference test). The pt^{pbs} group refers to the group in which mice were transplanted with the same dose of PBS after 3 days of IVH, and pt^{sham} group refers to the group in which mice underwent all surgical procedures without IVH and transplantation. IVH: Intraventricular hemorrhage; ns: not significant; NSC: neural stem cell; PBS: phosphate-buffered saline; pt: post-transplantation; Sox2: sex-determining region Y-box 2.

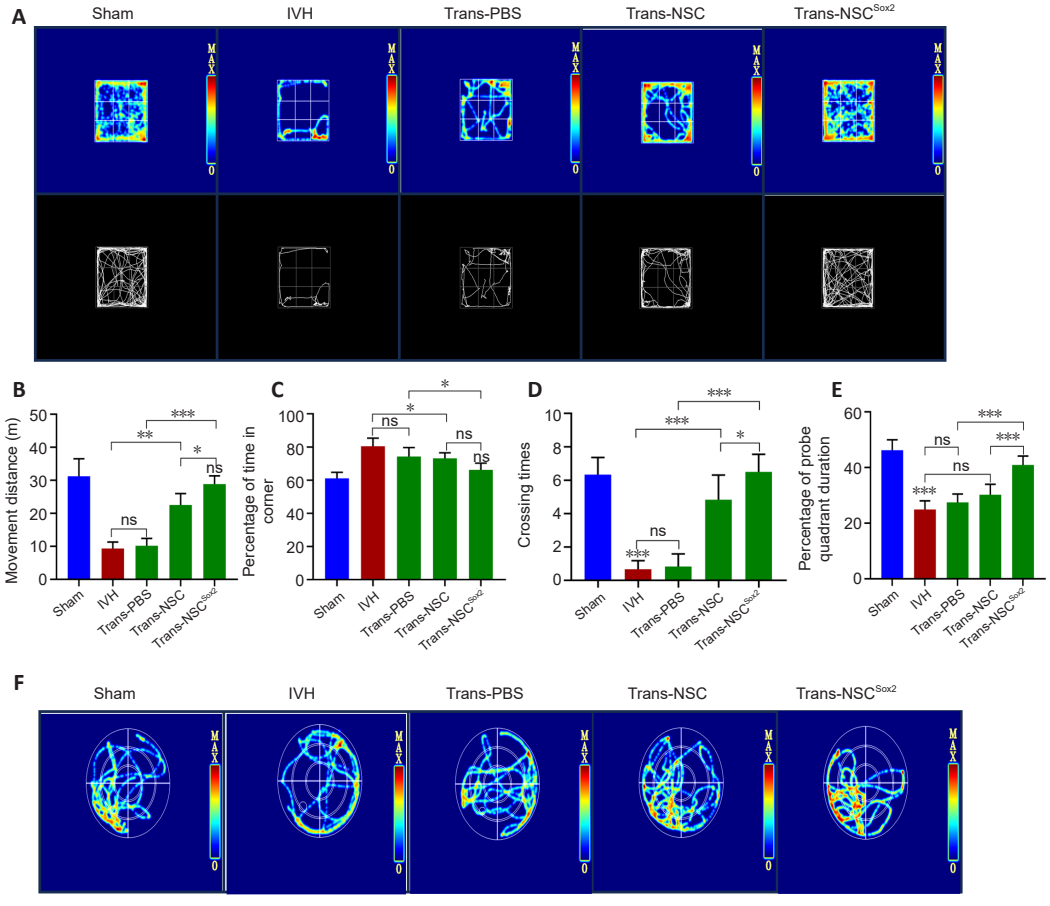

Figure 4 | NSC^{Sox2} transplantation improves neurocognitive functions in IVH mice.

(A) Representative tracing images from the open field test. (B) Quantification of the distance traveled for each group in the open field test. (C) Percent time spent in the corner zones for each group in the Morris water maze. (D) Number of crossings for each group. (E) Percent time spent in the probe quadrant for each group. All data are presented as the mean ± SD (n = 5). *P < 0.05, **P < 0.01, ***P < 0.001 (one-way analysis of variance followed by *post hoc* Tukey's honestly significant difference test). (F) Representative tracing images from the Morris water maze. IVH: Intraventricular hemorrhage; ns: not significant; NSC: neural stem cell; PBS: phosphate-buffered saline; pt: post-transplantation; Sox2: sex-determining region Y-box 2.

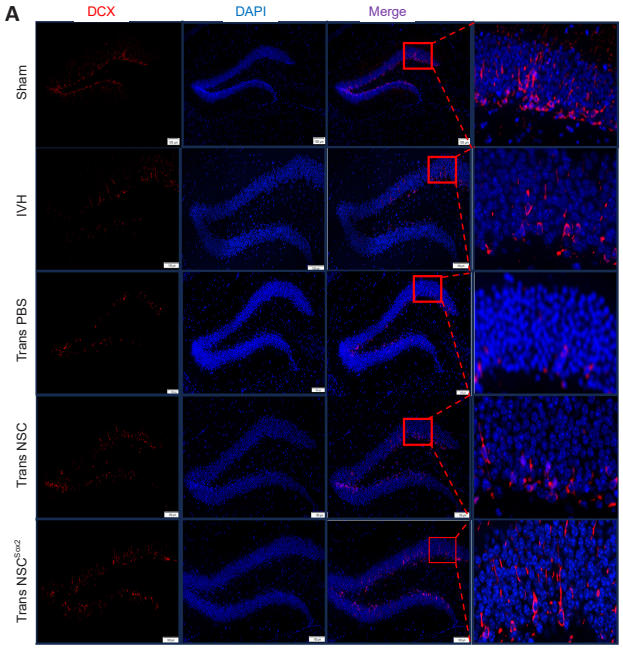

Figure 5 | NSC^{Sox2} transplantation upregulation of DCX expression in mouse hippocampus.

(A) Representative images of immunofluorescence staining for DCX (red, cyanine-3). Scale bars: 100 μm; enlarged images, 20 μm. (B) Relative fluorescence intensity of DCX. All data are presented as the mean ± SD (n = 5). $^{**}P < 0.01$, $^{***}P < 0.001$ (one-way analysis of variance followed by *post hoc* Tukey's honestly significant difference test). DAPI: 4′,6-Diamidino-2-phenylindole; DCX: doublecortin; IVH: intraventricular hemorrhage; ns: not significant; NSC: neural stem cell; PBS: phosphate-buffered saline; Sox2: sex-determining region Y-box 2.

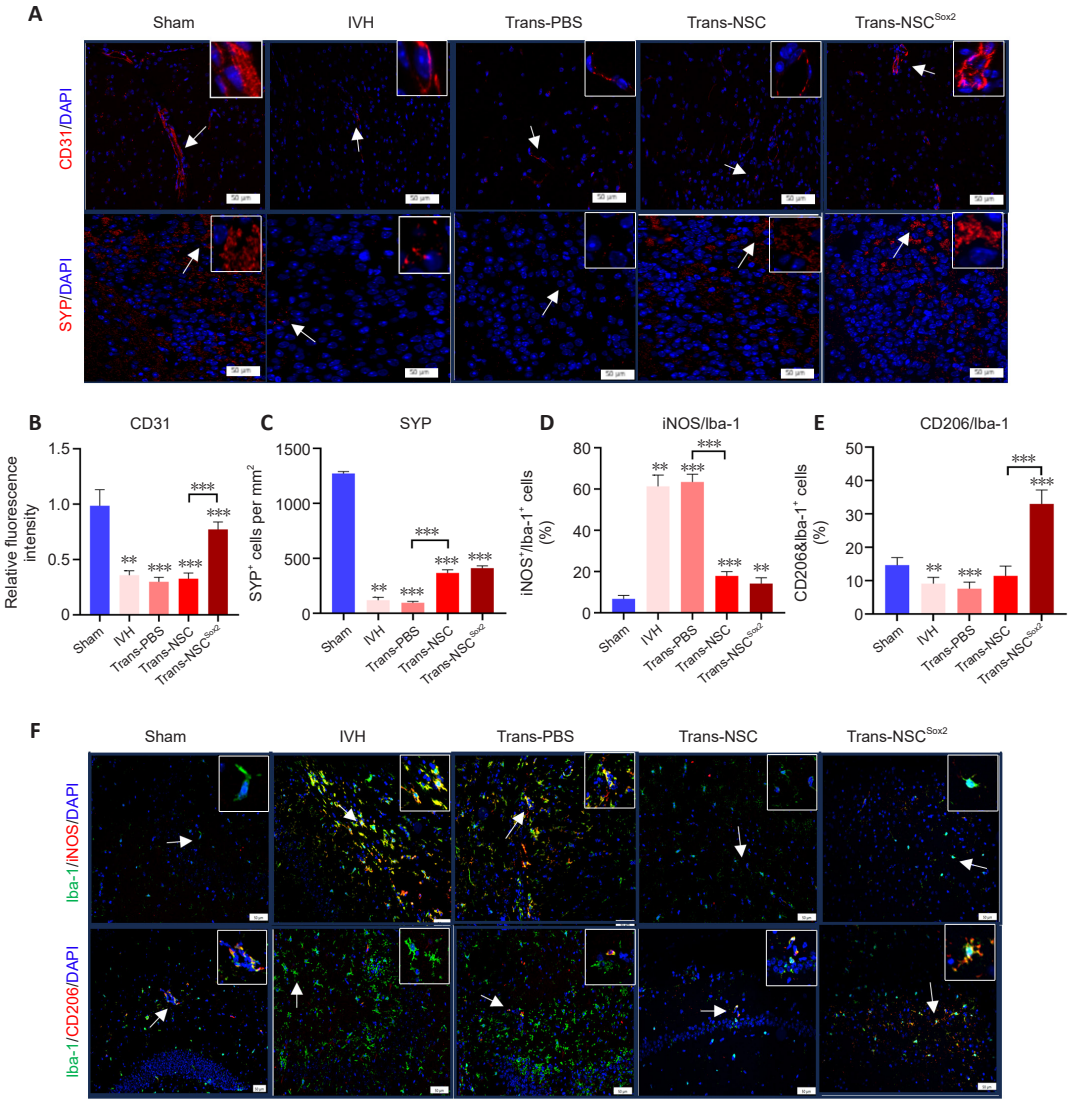

Figure 6 | NSC^{Sox2} transplantation promotes neurodegeneration, angiogenesis, and regulation of microglial polarization in mouse hippocampus.

(A) Representative images of immunofluorescence staining for CD31 (red, cyanine-3) and SYP (red, cyanine-3). (B) Statistical analysis of the relative fluorescence intensity of CD31 in A. (C) Statistical analysis of the relative fluorescence intensity of SYP in A. (D) Percentages of Iba-1- and iNOS-positive cells in F. (E) Percentages of Iba-1- and iNOS-positive cells in F. All data are presented as the mean ± SD (n = 5). $^{**}P < 0.01$, $^{***}P < 0.001$ (one-way analysis of variance followed by *post hoc* Tukey's honestly significant difference test). (F) Representative images of immunofluorescence staining for Iba-1 (green, CoraLite488)/iNOS (red, cyanine-3) and Iba-1 (green, CoraLite488)/CD206 (red, cyanine-3). Scale bars: 50 μm. The arrows indicate areas in insets. DAPI: 4′,6-Diamidino-2-phenylindole; Iba-1: ionized calcium-binding adapter molecule 1; iNOS: inducible nitric oxide synthase; IVH: intraventricular hemorrhage; NSC: neural stem cell; PBS: phosphate-buffered saline; Sox2: sex-determining region Y-box 2; SYP: synaptophysin.

NSC^{Sox2} transplantation attenuates intraventricular hemorrhage-induced TLR4 inflammatory SPAK-NKCC1-AQP-1 pathway activation in mice

Considering our findings that NSC^{Sox2} transplantation promoted the activation of M2 microglia to exert anti-inflammatory effects, and we next examined the protein expression of CSF-related signaling pathways in the choroid plexus before and after transplantation by western blot assay. Expression of Na-K-Cl cotransporter 1 (NKCC1) in the choroid plexus was increased after IVH ($P < 0.001$), and was highest 3 days after IVH, which was maintained at 1 week. NF-κB was highly expressed 2 weeks after IVH and aquaporin-1 (AQP-1) and Na^+/K^+ ATPase expression decreased after IVH ($P < 0.01$). Although serine-threonine STE20/SPS1-related proline-alanine-rich kinase (SPAK) and toll-like receptor 4 (TLR4) expression did not change significantly, we found an increase in phosphorylated serine/threonine protein kinase (p-SPAK) (**Figure 7A** and **B**). The NSC^{Sox2} group showed a similar trend (**Figure 7C** and **D**). We then compared protein expression in the IVH group, the PBS group and the NSC^{Sox2} group (**Figure 7E** and **F**). The gray values of NKCC1 normalized by GAPDH in sham group, IVH 3d, IVH 31d and NSC^{Sox2} groups (4 weeks post-transplantation) were 0.22 ± 0.04, 1.06 ± 0.14, 0.43 ± 0.03 and 0.26 ± 0.04, respectively, the results showed NKCC1 was highly expressed in the early stage of the IVH group, and had a tendency to decrease over time, and the NSC^{Sox2} group was the closest to the sham group. AQP-1 and Na^+/K^+ ATPase were decreased in the IVH group, and then gradually increased and were similar to the normal levels after 1 month. The highest expression of AQP-1 was found in the NSC^{Sox2} group, which could be related to the proliferation of choroid plexus epithelial cells after transplantation. Additionally, p-SPAK and NF-κB showed high expression after IVH, but were also abnormally increased in the PBS group, which could be due to a combined infection or other reasons (**Figure 7E** and **F**).

NSC^{Sox2} transplantation reduces the expression of proinflammatory factors while enhancing the expression of anti-inflammatory and neurotrophic factors in the hippocampus of intraventricular hemorrhage mice

We detected the expression of proinflammatory factors tumor necrosis factor-alpha (TNF-α) and interleukin (IL)-1β in the hippocampal region by ELISA (**Figure 8A** and **B**), and found that their expression levels were significantly increased after IVH ($P < 0.01$). NSC transplantation reduced their expression, and the decrease was greater with NSC^{Sox2} transplantation. The proinflammatory factors TNF-α and IL-6 and the anti-inflammatory factor IL-10 had low expression in the sham group (**Figure 8C** and **D**), and their expression increased after IVH. NSC transplantation reduced their expression levels, and the decrease was greater with NSC^{Sox2} transplantation. Additionally, we found that the expression of neurotrophic factors brain-derived growth factor (BDNF) and nerve growth factor (NGF) increased after transplantation of NSC and NSC^{Sox2}, and the expression of the same factors was shown to be higher in the NSC^{Sox2} group by western blot assay.

Discussion

We showed that $hNSC^{Sox2}$ transplantation led to significant behavioral improvements, reduced ventricular size compared with pre-transplantation size and substantial neural regeneration in the hippocampal region of PHH model mice. Additionally, we observed an increase in anti-inflammatory factors and a decrease in proinflammatory factors in CSF. These findings suggest that $hNSC^{Sox2}$ transplantation is both safe and effective for treating PHH.

In this study, we cultivated hNSC using fetal brain tissue and transfected Sox2 by lentivirus. Its sphere-forming rate and expansion rate increased significantly after transfection, the diameter of the cell spheres became larger, and the interval of fluid exchange also changed from 3–4 days before transfection to 1–2 days after transfection (data not shown), indicating that its self-renewal ability increased substantially. *In vitro* flow cytometric analysis of NSC and NSC^{Sox2} groups indicated that Sox2 promoted the proliferation of NSCs, and as the number of NSCs increased, so did the number of neurons that differentiated. This is consistent with the results in a previous study (Bertolini et al., 2019), which showed that after Sox2 knockdown *in vivo*, both SHH and Wnt, the key factors to maintain NSC proliferation, decreased significantly, resulting in impaired neural regeneration and reduced NSC number in the hippocampus.

For *in vitro* experiments, NSC^{Sox2} cells were cultured in differentiation medium with and without RA for 4 weeks. Flow cytometry showed that administration of RA increased the proportion of NSCs differentiating into neurons. Additionally, *in vivo* experiments 4 weeks after transplantation showed that the number of neurons increased significantly after NSC^{Sox2} transplantation and combined RA. These findings suggest that RA administration augmented the effect of NSC transplantation. This may be because the controlled release of RA from the osmotic pump would promote Wnt2b expression, enhance NeuroD1 and Prox1 expression, promote β-catenin synthesis, and thus promote the differentiation of NSC into neurons (Huang et al., 2021). RA upregulates the expression of NeuroD1, which is an important transcription factor for NSC differentiation into neurons (Gao et al., 2009). Upregulation of NeuroD1 was also shown to promote astrocyte reprogramming into neurons (Wang and Zhang, 2022).

We also found that the mean fluorescence intensity of DCX- and synaptophysin-positive cells were elevated in both transplanted NSCs and NSC^{Sox2} groups compared with the IVH group, suggesting that NSC transplantation had a substitution effect, and that NSC^{Sox2} transplantation was more efficacious. The newly generated neurons may originate from transplanted NSCs or from endogenous NSCs. The generation of endogenous neurons may be explained by multiple reasons. First, the anti-inflammatory effect produced by the transplanted NSCs may improve the local microenvironment and facilitate the survival and differentiation of endogenous NSCs. Second, the continuous administration of RA could promote the generation of endogenous neurons (Shibata et al., 2021). Third, even apoptotic transplanted NSCs can have neuroprotective effects by secreting peroxidedoxin-1 and galectin-1 (Karimy et al., 2020). However, a previous study showed that after RA was added to NSC medium, NSC markers, such as Sox2 and nestin, were decreased, S100β-positive cells were increased, and there was no significant correlation between neuronal markers ($NeuN^+$ and $MAP2^+$) and RA, which suggested that RA may be more likely to promote the differentiation of NSCs to astrocytes (Gong et al., 2023). In contrast, Kubickova et al. (2023) reported that the expression of neuronal protein increased with the increase of RA concentration. Here, we demonstrated through both *in vivo* and *in vitro* experiments that RA promoted the differentiation of NSCs into neurons, which suggests that RA promotes the differentiation of NSCs into both neurons and astrocytes (Chu et al., 2015).

We constructed a PHH model by intraventricular injection of autologous blood, which was confirmed by MRI to have enlarged ventricles and neurological deficits, both of which improved with NSC transplantation. PHH can cause ventricle enlargement and increased intracranial pressure, resulting in intracranial hypoxic-ischemic damage. This is followed by increased glycolysis, lipid peroxidation, oxidative stress, and activation of calcium-dependent proteolytic enzyme to destroy axons, which leads to axon stretching and destruction, and reduced connections between neurons (Kahle et al., 2016, 2024). Further, electrophysiological assays have documented attenuation of long duration enhancement in hippocampal neurons, suggesting that the postsynaptic integration process is disrupted (Yin et al., 2018). We chose the hippocampal dentate gyrus region for transplantation because this is one of the two regions in which NSCs reside and is an important site for neurogenesis (Vicidomini et al., 2020). Additionally, previous findings suggest that Sox2 expression is more sensitive to NSC proliferation and neural regeneration in the hippocampal region than in the subventricular zone (Favaro et al., 2009). Because ventricular enlargement causes the hippocampal position to shift after the occurrence of PHH, we used the following target coordinates relative to bregma: $x = 2.5$ mm, $y = -2.0$ mm, $z = -2.2$ mm. MRI images and fluorescence imaging of postoperative tissue sections showed that the graft was located in the hippocampal region.

For ventricle enlargement after IVH, we found that the first sharp enlargement of the ventricles appeared 3 days after modeling. Although a previous study showed that CSF secretion in the choroid plexus is high during 1–7 days after IVH (McAllister et al., 2017), we thought that the sharp enlargement of the ventricles at this time was mainly due to obstruction. Then, 1 to 2 weeks after IVH, the ventricles slowly enlarged and temporarily shrunk, which was possibly due to obstruction relief after hematoma absorption and the decrease of CSF secretion due to a sharp increase in intracranial pressure (Holste et al., 2024). At 3 weeks after IVH, the enlargement of the ventricles may be due to the formation of ventricular scars, fibrosis, or arachnoid scars that led to damage of lymphatic pathways, which would in turn lead to the obstruction of CSF circulatory pathways. We chose 3 days after IVH for cell transplantation because the PHH mice often showed cognitive and motor deficits at this time point. Moreover, it has also been shown that early

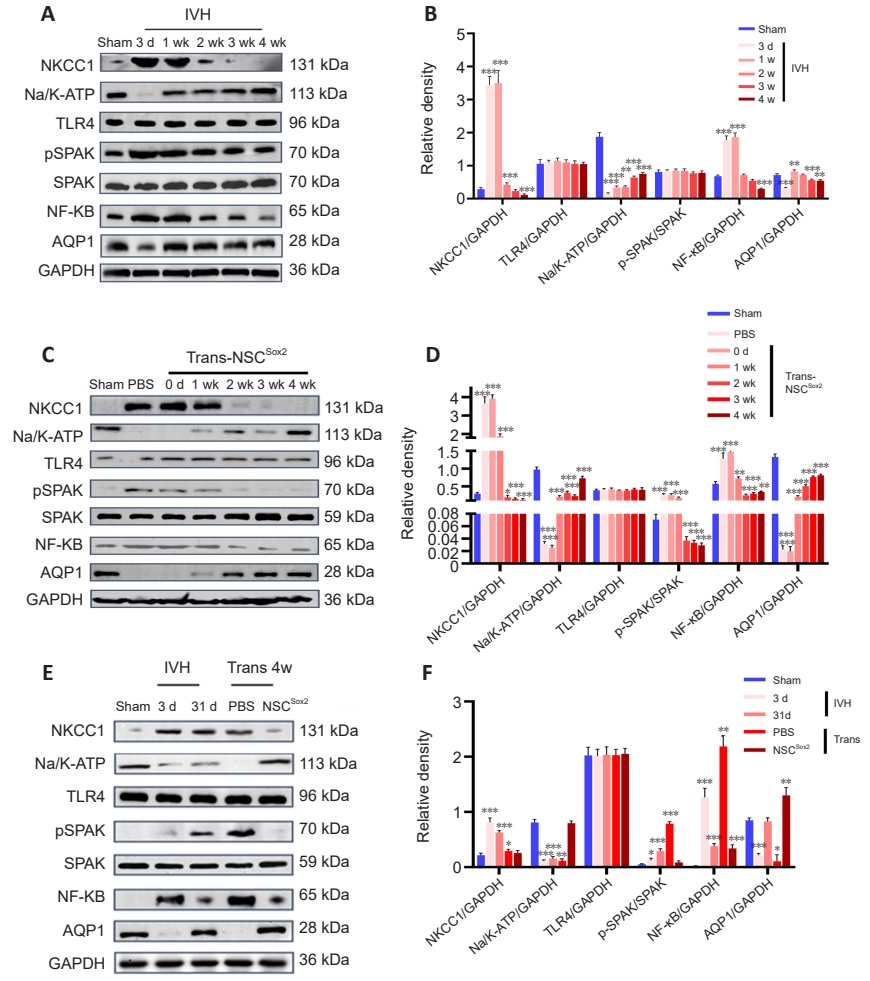

Figure 7 | NSC^{Sox2} transplantation attenuates IVH-activated TLR4 inflammatory SPAK-NKCC1-AQP-1 pathway in mouse choroid plexus.

(A) Typical western blot bands of NKCC1, Na/ATP, TLR4, SPAK, NF-κB and AQP-1 in IVH. (B) Statistical analysis of proteins in each group. (C) Typical western blot bands of NKCC1, Na/ATP, TLR4, SPAK, NF-κB and AQP-1 in sham and post-transplantation groups. (D) Statistical analysis of proteins. (E) Typical western blot bands of NKCC1, Na/ATP, TLR4, SPAK, NF-κB and AQP-1. (F) Statistical analysis of proteins in each group. All data are presented as the mean ± SD (n = 5). *P < 0.05, **P < 0.01, ***P < 0.001, *vs*. Sham group (one-way analysis of variance followed by *post hoc* Tukey's honestly significant difference test). AQP-1: Aquaporin-1; IVH: intraventricular hemorrhage; Na/ATP: Na^+/K^+ ATPase; NF-κB: nuclear factor-κB; NKCC1: Na-K-Cl cotransporter 1; NSC: neural stem cell; PBS: phosphate-buffered saline; p-SPAK: phosphorylated serine/threonine protein kinase; SD: standard deviation; Sox2: sex-determining region Y-box 2; SPAK: SPS1-related proline-alanine-rich kinase; TLR4: toll-like receptor 4.

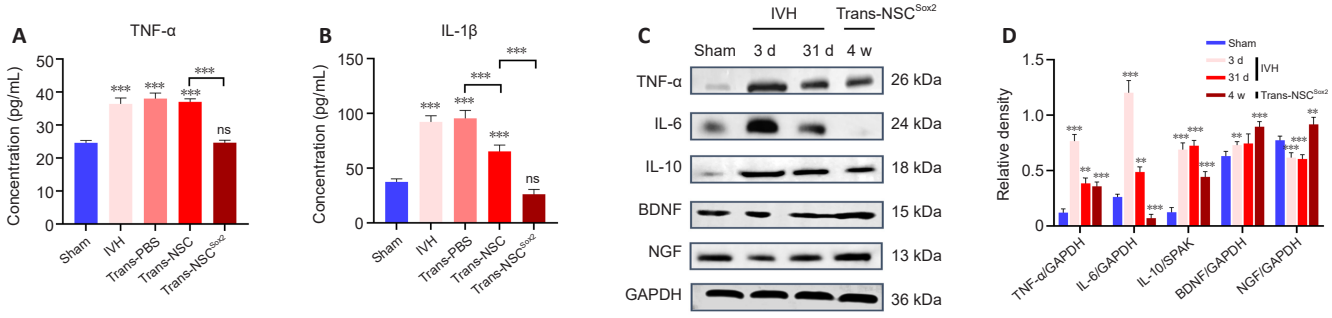

Figure 8 | NSC^{Sox2} transplantation decreases the expression of proinflammatory factors and increases the expression of anti-inflammatory factors and neurotrophic factors in hippocampus.

(A, B) ELISA results of TNF-α (A) and IL-1β (B) in hippocampus. (C) Typical western blot bands of TNF-α, IL-6, IL-10, BDNF, and NGF. (D) Statistical analysis of proteins. All data are presented as the mean ± SD (n = 5). **P < 0.01, ***P < 0.001, *vs*. Sham group (one-way analysis of variance followed by *post hoc* Tukey's honestly significant difference test). BDNF: Brain-derived growth factor; ELISA: enzyme-linked immunosorbent assay; GAPDH: glyceraldehyde-3-phosphate dehydrogenase; IL: interleukin; IVH: intraventricular hemorrhage; NGF: nerve growth factor; NSC: neural stem cell; PBS: phosphate-buffered saline; SD: standard deviation; Sox2: sex-determining region Y-box 2; TNF-α: tumor necrosis factor-alpha.

transplantation is most effective in ischemia and hypoxia caused by increased intracranial pressure due to hydrocephalus (Wang et al., 2024). In that study, transplantation within 48 hours of the onset of cerebral ischemia and hypoxia resulted in a significantly higher NSC survival rate than transplantation after 6 weeks, although theoretically, transplantation after inflammation has subsided is more likely to increase NSC survival rate (Wang et al., 2024). In the present study, we found that early transplantation significantly enhanced endogenous repair mechanisms, such as axonal plasticity, angiogenesis and neuroprotection. Moreover, it has been shown that interventions early after PHH result in lower rates of patient mortality and severe neurological deficits, whereas intervention when the patient's condition has worsened results in a significantly worse prognosis (Cizmeci et al., 2020).

In this study, we found that the numbers of hippocampal DCX$^+$ cells and synaptophysin fluorescence intensity in the transplanted NSC and NSC^{Sox2} groups were significantly higher than those in the IVH group, suggesting that the transplanted cells survived and established synaptic connections with the graft. These findings indicate an increase in neural regeneration in the hippocampal area. A previous study reported that the number of newly generated immature neurons was significantly positively correlated with cognitive scores, and more DCX$^+$ cells was associated with better cognitive ability (Tobin et al., 2019). Using immunofluorescence, we also detected new blood vessels in the hippocampus growing to the grafted area within 1 month after NSC transplantation. Immunofluorescence staining also suggested that angiogenesis increased over time, which may be due to the fact that NSC

transplantation can induce increased secretion of vascular endothelial growth factor and promote the regeneration of blood vessels by activating the JAK2/STAT3 signaling pathway (Zhang et al., 2019). It has also been shown that angiogenesis and neural regeneration may share some of the same signaling pathways, such as stromal cell-derived factor-1 and angiopoietin-1 (Paro et al., 2023). Moreover, it was shown that even a small number of surviving transplanted NSCs secrete trophic factors to repair tissue damage through paracrine effects (Xiong et al., 2021). We detected the neuroprotective factors BDNF and NGF in the hippocampus by western blot assay and found that expression in the PHH group decreased over time, and that NSC^{Sox2} transplantation reversed this phenomenon. A previous study showed that NSCs promote the expression of chemokine receptors and adhesion molecules under the action of BDNF (Sortino et al., 2024), which is conducive to the migration of NSC and tissue repair (Yang et al., 2022). Additionally, transplanted NSCs may stimulate the proliferation and migration of endogenous NSCs by secreting fibroblast growth factor 2, insulin-like growth factor, BDNF, vascular endothelial growth factor and chemokines (e.g., matrix metalloproteinase and monocyte chemotactic protein-1) (Wang et al., 2024). Neurons differentiated from transplanted NSCs also extended axons and formed synapses from the injury site, thereby supporting neurological repair (Wang et al., 2024). Finally, through the water maze and open field tests, we found that both NSC and NSC^{Sox2} transplantation improved the neurological dysfunction of PHH mice, and that the effect of NSC^{Sox2} transplantation was greater.

Microglia are intrinsic immune cells within the central nervous system and have three phenotypes, M1 (characterized by amoeboid bodies), intermediate and M2 (characterized by long, bifurcated protrusions), that shift in response to changes in the environment (Guerrero and Sicotte, 2020). The intermediate phenotype can be activated into the M1 phenotype after interferon-γ or lipopolysaccharide stimulation, which then secretes proinflammatory factors (e.g. glutamate, reactive oxygen species and nitric oxide) that contribute to neurodegeneration. Microglia can also be stimulated by IL-4 or IL-13 to M2-type activation, which upregulates the expression of regeneration factors, such as Arg1. We found that the IVH group had a significant increase in M1-type $iNOS^{+}$/Iba-1^{+} cells and a significant decrease in M2-type $CD206^{+}$/Iba-1^{+} cells, which was rescued by transplantation of NSC^{Sox2}. We also detected inflammatory factors in the hippocampal region by ELISA and found low levels of proinflammatory factors in the sham group. In the IVH group, both TNF-α and IL-1β were significantly increased compared with those in the sham group. Transplanted NSC and NSC^{Sox2} reduced their expression in IVH mice ($P < 0.001$), and the effect was greater with transplanted NSC^{Sox2}. Western blot assay showed similar changes in TNF-α and IL-6, and showed that the anti-inflammatory factor IL-10 was increased after transplantation. These findings suggest that transplanted NSCs exerted an immunomodulatory effect for at least 30 days, promoting M2 phenotype activation, reducing the expression of proinflammatory factors TNF-α, IL-1β and IL-6, downregulating M1 phenotype microglia activity, maintaining blood–brain barrier permeability, and reducing the inflammatory waterfall cascade response (Lockard et al., 2022). A previous study showed that the levels of inflammatory factors, such as IL-6, IL-4, TNF-α and TGF-β1, in the peripheral blood or CSF correlated with hydrocephalus symptoms, and in particular were positively correlated with cognitive deficits (Thwaites et al., 2007). Further, targeted therapy of inflammatory pathway molecules has been shown to restore the abnormal secretion state of the choroid plexus, ependymal stripping, tissue injury and scar formation of the ventricle wall and glymphatic system (Karimy et al., 2020). The findings here indicate that NSC transplantation reduces the concentration of inflammatory factors in brain tissue, thus improving the clinical symptoms of PHH.

We found that the PHH model induced by IVH resulted in increased proinflammatory factors, which can lead to ventricular wall fibrosis and ependymal detachment, and in turn can cause reactive gliosis, destroy the lymphatic circulation pathway and then aggravate hydrocephalus (Ding et al., 2019). However, abnormal CSF secretion by the choroid plexus, rather than impaired lymphatic circulation, is the main factor leading to hydrocephalus (McAllister et al., 2017). The ability of the choroid plexus to produce CSF is dynamically regulated by inflammation, known as immune-secretory plasticity, which is one of the important pathological mechanisms of PHH. In rodents, approximately 80% of CSF is produced by the choroid plexus (Steffensen et al., 2018). The remaining CSF may be derived from the brain interstitial fluid. Therefore, we examined the expression of proteins related to the SPAK-NKCC1-AQP-1 signaling pathway associated with CSF secretion by choroid plexus tissues before and after transplantation. NF-κB, NKCC1, Na/K-ATP and AQP-1 were significantly increased 3–7 days after IVH. It is possible that blood metabolites, such as methemoglobin and ferric ions, bind to TLR4 receptors on the surface of choroid plexus cells (Kwon et al., 2015), which activate the NF-kB signaling pathway and promote the secretion of inflammatory factors (e.g. TNF-α and IL-1), and regulate SPAK. SPAK integrates and converts information from the surrounding environment, such as NF-kB and its regulated inflammatory factors including TNF-α, IL-1β and INF-γ (Karimy et al., 2020), and phosphorylates the NKCC1 cotransporter on the parietal membrane of the choroid plexus. This then opens AQP-1 on the CSF side of choroidal epithelial cells, forming an osmotic pressure gradient that drives CSF from the blood to the cerebral ventricle. It was previously reported that NF-κB activation increased the rate of CSF secretion from the choroid plexus epithelium by more than 3-fold (Karimy et al., 2017). In the present study, we found that NSC^{Sox2} transplantation reduced the expression of proteins related to this signaling pathway, which suggests that NSC^{Sox2} transplantation slowed down CSF hypersecretion by the choroid plexus, thereby reversing ventricle enlargement and the symptoms related to hydrocephalus. Therefore, we believe that targeted treatment of inflammation in the choroid plexus would not only resolve CSF hypersecretion in the choroid plexus, but also block the secondary tissue damage caused by inflammation. Focusing on inflammation allows us to shift the perception of hydrocephalus as a lifelong neurological disorder to a preventable neuroinflammatory disorder.

Overall, because of the complexity of the pathological mechanisms of PHH, it is particularly important to develop multifunctional therapeutic modalities that can simultaneously address multiple pathological mechanisms. This is the first time that NSC^{Sox2} transplantation was applied in combination with RA to treat PHH. We found that transplanted NSC^{Sox2} survived in PHH mice, differentiated into new neurons *in vivo* to exert a substitution effect and secreted trophic factors to promote neural regeneration and angiogenesis, and promoted the activation of M2 microglia to exert an anti-inflammatory effect. Further, behavioral tests showed that NSC^{Sox2} significantly improved neurological dysfunction in PHH model mice (Vorhees and Williams, 2006). However, NSC transplantation has some limitations. Firstly, NSCs are difficult to acquire clinically because of ethical and other complications, and their quantity is small. In contrast, induced pluripotent stem cells are easy to obtain, have low immunogenicity, and are susceptible to gene editing (Jing et al., 2022; Marei et al., 2023). Thus, whether induced pluripotent stem cells would be effective should be investigated in future studies. Secondly, because of the ventricular enlargement after PHH, which worsens over time, the hippocampal position could not be precisely located due to individual variation. Therefore, ultrasound-guided transplantation may be helpful. Alternatively, whether NSCs could be transplanted via intraventricular or transnasal routes needs to be determined by further experiments. Thirdly, it has been shown that *in vivo* transplanted NSCs differentiate into neurons within 2 months and into glial cells within 4 months after transplantation (Xu et al., 2024). Therefore, the long-term effects of NSC transplantation on PHH still needs to be studied. Lastly, in the present study, we excluded female mice to account for the potential influence of estrogen. Thus, we must acknowledge that this limits the generalizability of our findings.

Author contributions: *Definition of intellectual content, literature search, data analysis, statistical analysis, manuscript preparation, manuscript editing & manuscript review: BG, HW and SH. Data acquisition and manuscript review: KZ, XL, ZD and YL. Definition of intellectual content, data acquisition, data analysis, statistical analysis, manuscript editing & manuscript review: LZ and AT. All authors reviewed the results and approved the final version of the manuscript.*
Conflicts of interest: *The authors declare no conflicts of interest.*
Data availability statement: *All data relevant to the study are included in the article or uploaded as Additional files.*

Open peer reviewers: *Juan F. Villalonga, National University of Tucumán, Argentina; Hao Tang, University of Leicester, UK.*
Additional files:
Additional Table 1: *List of the antibodies used in this study.*
Additional file 1: *Open peer review reports 1 and 2.*

References

Baloh RH, et al. (2022) Transplantation of human neural progenitor cells secreting GDNF into the spinal cord of patients with ALS: A phase 1/2a trial. Nat Med 28:1813-1822.
Bertolini JA, et al. (2019) Mapping the global chromatin connectivity network for Sox2 function in neural stem cell maintenance. Cell Stem Cell 24:462-476.e6.
Cao Y, Liu C, Li G, Gao W, Tang H, Fan S, Tang X, Zhao L, Wang H, Peng A, You C, Tong A, Zhou L (2023) Metformin alleviates delayed hydrocephalus after intraventricular hemorrhage by inhibiting inflammation and fibrosis. Transl Stroke Res 14:364-382.
Chiang WW, Takoudis CG, Lee SH, Weis-McNulty A, Glick R, Alperin N (2009) Relationship between ventricular morphology and aqueductal cerebrospinal fluid flow in healthy and communicating hydrocephalus. Invest Radiol 44:192-199.
Chu T, Zhou H, Wang T, Lu L, Li F, Liu B, Kong X, Feng S (2015) In vitro characteristics of valproic acid and all-trans-retinoic acid and their combined use in promoting neuronal differentiation while suppressing astrocytic differentiation in neural stem cells. Brain Res 1596:31-47.
Cizmeci MN, Groenendaal F, Liem KD, van Haastert IC, Benavente-Fernández I, van Straaten HLM, Steggerda S, Smit BJ, Whitelaw A, Woerdeman P, Heep A, de Vries LS (2020) Randomized controlled early versus late ventricular intervention study in posthemorrhagic ventricular dilatation: outcome at 2 years. J Pediatr 226:28-35.e3.
Ding Y, Zhang T, Wu G, McBride DW, Xu N, Klebe DW, Zhang Y, Li Q, Tang J, Zhang JH (2019) Astrogliosis inhibition attenuates hydrocephalus by increasing cerebrospinal fluid reabsorption through the glymphatic system after germinal matrix hemorrhage. Exp Neurol 320:113003.
Dong Y, Xu T, Yuan L, Wang Y, Yu S, Wang Z, Chen S, Chen C, He W, Stewart T, Zhang W, Yang X (2024) Cerebrospinal fluid efflux through dynamic paracellular pores on venules as a missing piece of the brain drainage system. Exploration (Beijing) 4:20230029.
Favaro R, Valotta M, Ferri AL, Latorre E, Mariani J, Giachino C, Lancini C, Tosetti V, Ottolenghi S, Taylor V, Nicolis SK (2009) Hippocampal development and neural stem cell maintenance require Sox2-dependent regulation of Shh. Nat Neurosci 12:1248-1256.
Fedorov A, Beichel R, Kalpathy-Cramer J, Finet J, Fillion-Robin JC, Pujol S, Bauer C, Jennings D, Fennessy F, Sonka M, Buatti J, Aylward S, Miller JV, Pieper S, Kikinis R (2012) 3D Slicer as an image computing platform for the Quantitative Imaging Network. Magn Reson Imaging 30:1323-1341.
Gao Z, Ure K, Ables JL, Lagace DC, Nave KA, Goebbels S, Eisch AJ, Hsieh J (2009) Neurod1 is essential for the survival and maturation of adult-born neurons. Nat Neurosci 12:1090-1092.
Garcia-Bonilla M, Castaneyra-Ruiz L, Zwick S, Talcott M, Otun A, Isaacs AM, Morales DM, Limbrick DD, Jr., McAllister JP, 2nd (2022) Acquired hydrocephalus is associated with neuroinflammation, progenitor loss, and cellular changes in the subventricular zone and periventricular white matter. Fluids Barriers CNS 19:17.
Gong Y, Liu Z, Zhou P, Li J, Miao YB (2023) Biomimetic nanocarriers harnessing microbial metabolites usher the path for brain disease therapy. Nano TransMed 2:100020.
Gonzalo Domínguez M, Hernández C, Ruisoto P, Juanes JA, Prats A, Hernández T (2016) Morphological and volumetric assessment of cerebral ventricular system with 3D Slicer software. J Med Syst 40:154.
Guerrero BL, Sicotte NL (2020) Microglia in multiple sclerosis: Friend or foe? Front Immunol 11:374.
Hersh DS, Kumar R, Klimo P, Bookland M, Martin JE (2021) Hydrocephalus surveillance following shunt placement or endoscopic third ventriculostomy: a survey of surgeons in the Hydrocephalus Clinical Research Networks. J Neurosurg Pediatr 28:139-146.
Holste KG, Ye F, Koduri S, Garton HJL, Maher CO, Keep RF, Hua Y, Xi G (2024) Attenuation of ventriculomegaly and iron overload after intraventricular hemorrhage by membrane attack complex inhibition. J Neurosurg 140:1482-1492.
Huang D, Cao Y, Yang X, Liu Y, Zhang Y, Li C, Chen G, Wang Q (2021) A nanoformulation-mediated multifunctional stem cell therapy with improved beta-amyloid clearance and neural regeneration for Alzheimer's disease. Adv Mater 33:e2006357.
Jeong I, Jurisch-Yaksi N (2023) Boosting NKCC1 in the choroid plexus: From CSF clearance to a potential therapy for posthemorrhagic hydrocephalus. Neuron 111:1521-1523.
Ji X, Zhou Y, Gao Q, He H, Wu Z, Feng B, Mei Y, Cheng Y, Zhou W, Chen Y, Xiong M (2023) Functional reconstruction of the basal ganglia neural circuit by human striatal neurons in hypoxic-ischaemic injured brain. Brain 146:612-628.
Jing S, Zhou H, Zou C, Chen DPC, Ye Q, Ai Y, He Y (2022) Application of telomere biology and telomerase in mesenchymal stem cells. Nano TransMed 1:e9130007.
Kahle KT, Kulkarni AV, Limbrick DD, Jr., Warf BC (2016) Hydrocephalus in children. Lancet 387:788-799.
Kahle KT, Klinge PM, Koschnitzky JE, Kulkarni AV, MacAulay N, Robinson S, Schiff SJ, Strahle JM (2024) Paediatric hydrocephalus. Nat Rev Dis Primers 10:35.
Karimy JK, Reeves BC, Damisah E, Duy PQ, Antwi P, David W, Wang K, Schiff SJ, Limbrick DD, Jr., Alper SL, Warf BC, Nedergaard M, Simard JM, Kahle KT (2020) Inflammation in acquired hydrocephalus: pathogenic mechanisms and therapeutic targets. Nat Rev Neurol 16:285-296.
Karimy JK, Zhang J, Kurland DB, Theriault BC, Duran D, Stokum JA, Furey CG, Zhou X, Mansuri MS, Montejo J, Vera A, DiLuna ML, Delpire E, Alper SL, Gunel M, Gerzanich V, Medzhitov R, Simard JM, Kahle KT (2017) Inflammation-dependent cerebrospinal fluid hypersecretion by the choroid plexus epithelium in posthemorrhagic hydrocephalus. Nat Med 23:997-1003.
Kubickova B, Martinkova S, Bohaciakova D, Nezvedova M, Liu R, Brozman O, Spáčil Z, Hilscherova K (2023) Effects of all-trans and 9-cis retinoic acid on differentiating human neural stem cells in vitro. Toxicology 487:153461.
Kwon MS, Woo SK, Kurland DB, Yoon SH, Palmer AF, Banerjee U, Iqbal S, Ivanova S, Gerzanich V, Simard JM (2015) Methemoglobin is an endogenous toll-like receptor 4 ligand-relevance to subarachnoid hemorrhage. Int J Mol Sci 16:5028-5046.
Li Y, Di C, Song S, Zhang Y, Lu Y, Liao J, Lei B, Zhong J, Guo K, Zhang N, Su S (2023) Choroid plexus mast cells drive tumor-associated hydrocephalus. Cell 186:5719-5738.e28.
Liu G, Ladrón-de-Guevara A, Izhiman Y, Nedergaard M, Du T (2022) Measurements of cerebrospinal fluid production: A review of the limitations and advantages of current methodologies. Fluids Barriers CNS 19:101.
Lockard GM, Alayli A, Monsour M, Gordon J, Schimmel S, Elsayed B, Borlongan CV (2022) Probing interleukin-6 in stroke pathology and neural stem cell transplantation. Int J Mol Sci 23:15453.
MacAulay N (2021) Molecular mechanisms of brain water transport. Nat Rev Neurosci 22:326-344.
Marei HE, Khan MUA, Hasan A (2023) Potential use of iPSCs for disease modeling, drug screening, and cell-based therapy for Alzheimer's disease. Cell Mol Biol Lett 28:98.
McAllister JP, Guerra MM, Ruiz LC, Jimenez AJ, Dominguez-Pinos D, Sival D, den Dunnen W, Morales DM, Schmidt RE, Rodriguez EM, Limbrick DD (2017) Ventricular zone disruption in human neonates with intraventricular hemorrhage. J Neuropathol Exp Neurol 76:358-375.
National Research Council (2011) Guide for the Care and Use of Laboratory Animals, 8th edition. Washington, DC, USA: National Academies Press.
No authors listed (1841) Acute hydrocephalus, or water in the head, an inflammatory disease, and curable equally and by the same means with other diseases of inflammation. Br Foreign Med Rev 11:151-158.
Pagin M, Pernebrink M, Giubbolini S, Barone C, Sambruni G, Zhu Y, Chiara M, Ottolenghi S, Pavesi G, Wei CL, Cantù C, Nicolis SK (2021) Sox2 controls neural stem cell self-renewal through a Fos-centered gene regulatory network. Stem Cells 39:1107-1119.
Park HJ, Jeon J, Choi J, Kim JY, Kim HS, Huh JY, Goldman SA, Song J (2021) Human iPSC-derived neural precursor cells differentiate into multiple cell types to delay disease progression following transplantation into YAC128 Huntington's disease mouse model. Cell Prolif 54:e13082.
Paro MR, Chakraborty AR, Angelo S, Nambiar S, Bulsara KR, Verma R (2023) Molecular mediators of angiogenesis and neurogenesis after ischemic stroke. Rev Neurosci 34:425-442.
Rajendran A, Rajan RA, Balasubramaniyam S, Elumalai K (2025) Nano delivery systems in stem cell therapy: Transforming regenerative medicine and overcoming clinical challenges. Nano TransMed 4:100069.
Schneider CA, Rasband WS, Eliceiri KW (2012) NIH Image to ImageJ: 25 years of image analysis. Nat Methods 9:671-675.
Sheikh AM, Hossain S, Tabassum S (2024) Advances in stem cell therapy for stroke: mechanisms, challenges, and future directions. Regen Med Rep 1:76-92.
Shibata M, Pattabiraman K, Lorente-Galdos B, Andrijevic D, Kim SK, Kaur N, Muchnik SK, Xing X, Santpere G, Sousa AMM, Sestan N (2021) Regulation of prefrontal patterning and connectivity by retinoic acid. Nature 598:483-488.
Sortino M, Amato A, Musumeci G (2024) Advanced technologies applied to physical exercise for dementia and Alzheimer's disease management: a narrative review. Adv Technol Neurosci 1:72-85.
Steffensen AB, Oernbo EK, Stoica A, Gerkau NJ, Barbuskaite D, Tritsaris K, Rose CR, MacAulay N (2018) Cotransporter-mediated water transport underlying cerebrospinal fluid formation. Nat Commun 9:2167.
Temple S (2023) Advancing cell therapy for neurodegenerative diseases. Cell Stem Cell 30:512-529.
Thwaites GE, Macmullen-Price J, Tran TH, Pham PM, Nguyen TD, Simmons CP, White NJ, Tran TH, Summers D, Farrar JJ (2007) Serial MRI to determine the effect of dexamethasone on the cerebral pathology of tuberculous meningitis: an observational study. Lancet Neurol 6:230-236.
Tobin MK, Musaraca K, Disouky A, Shetti A, Bheri A, Honer WG, Kim N, Dawe RJ, Bennett DA, Arfanakis K, Lazarov O (2019) Human hippocampal neurogenesis persists in aged adults and Alzheimer's disease patients. Cell Stem Cell 24:974-982.e3.
Vicidomini C, Guo N, Sahay A (2020) Communication, cross talk, and signal integration in the adult hippocampal neurogenic niche. Neuron 105:220-235.
Vorhees CV, Williams MT (2006) Morris water maze: procedures for assessing spatial and related forms of learning and memory. Nat Protoc 1:848-858.
Wang LL, Zhang CL (2022) In vivo glia-to-neuron conversion: pitfalls and solutions. Dev Neurobiol 82:367-374.
Wang S, He Q, Qu Y, Yin W, Zhao R, Wang X, Yang Y, Guo ZN (2024) Emerging strategies for nerve repair and regeneration in ischemic stroke: neural stem cell therapy. Neural Regen Res 19:2430-2443.
Wei JP, Wen W, Dai Y, Qin LX, Wen YQ, Duan DD, Xu SJ (2021) Drinking water temperature affects cognitive function and progression of Alzheimer's disease in a mouse model. Acta Pharmacol Sin 42:45-54.
Xiong M, Tao Y, Gao Q, Feng B, Yan W, Zhou Y, Kotsonis TA, Yuan T, You Z, Wu Z, Xi J, Haberman A, Graham J, Block J, Zhou W, Chen Y, Zhang SC (2021) Human stem cell-derived neurons repair circuits and restore neural function. Cell Stem Cell 28:112-126.e6.
Xu SB, Li XR, Fan P, Li X, Hong Y, Han X, Wu S, Chu C, Chen Y, Xu M, Lin M, Guo X, Liu Y (2024) Single-cell transcriptome landscape and cell fate decoding in human brain organoids after transplantation. Adv Sci (Weinh) 11:e2402287.
Yang H, Han M, Li J, Ke H, Kong Y, Wang W, Wang L, Ma W, Qiu J, Wang X, Xin T, Liu H (2022) Delivery of miRNAs through metal-organic framework nanoparticles for assisting neural stem cell therapy for ischemic stroke. ACS Nano 16:14503-14516.
Yin LK, Zheng JJ, Tian JQ, Hao XZ, Li CC, Ye JD, Zhang YX, Yu H, Yang YM (2018) Abnormal gray matter structural networks in idiopathic normal pressure hydrocephalus. Front Aging Neurosci 10:356.
Zhang T, Ke W, Zhou X, Qian Y, Feng S, Wang R, Cui G, Tao R, Guo W, Duan Y, Zhang X, Cao X, Shu Y, Yue C, Jing N (2019) Human neural stem cells reinforce hippocampal synaptic network and rescue cognitive deficits in a mouse model of Alzheimer's disease. Stem Cell Reports 13:1022-1037.
Zhang W, Chen H, Ding L, Huang J, Zhang M, Liu Y, Ma R, Zheng S, Gong J, Piña-Crespo JC, Zhang Y (2023) Microglial targeted therapy relieves cognitive impairment caused by Cntnap4 deficiency. Exploration (Beijing) 3:20220160.

P-Reviewers: Villalonga JF, Tang H; C-Editor: Zhao M; S-Editors: Yu J, Li CH; L-Editors: McCollum L, Yu J, Song LP; T-Editor: Jia Y

过表达 Sox2 的神经干细胞减轻出血后脑积水中的脑室扩大和神经功能障碍
文章特色分析

一、文章重要性

1. 临床问题突出：

出血后脑积水（PHH）是早产儿和成人脑室内出血后的常见并发症，目前主要依赖脑脊液分流术等手术治疗，但存在高失败率、多次手术及不可逆神经损伤等问题。本研究提出一种细胞治疗策略，有望弥补现有治疗的不足。

2. 治疗机制深入：

研究不仅验证了神经干细胞（NSCs）移植的可行性，还通过基因工程手段增强其存活与分化能力，并联合视黄酸（RA）促进神经再生与抗炎反应，系统性地干预了 PHH 的多重病理环节。

3. 转化潜力显著：

研究在动物模型中证实了 NSC 移植能改善脑室扩大、认知与运动功能，并揭示了其作用机制，为临床转化提供了理论依据和实验基础。

二、文章创新性特色

1. 基因工程联合药物干预：

- 首次将过表达 Sox2 的人源神经干细胞（NSC^Sox2） 与持续释放的视黄酸（RA） 联合应用于 PHH 治疗。

- Sox2 增强 NSC 的自我更新与增殖能力，RA 促进其向神经元分化，二者协同作用，显著提升治疗效果。

2. 多机制协同治疗：

- 神经再生：增加 DCX+神经元前体细胞和 NeuN+成熟神经元。

- 抗炎与免疫调节：促进小胶质细胞向 M2 型（抗炎型）极化，降低促炎因子（TNF-α, IL-1β, IL-6），提高抗炎因子（IL-10）。

- 血管生成与突触重建：提升 CD31（血管标志）和 SYP（突触标志）表达。

- 调控脑脊液分泌：通过抑制 TLR4–SPAK–NKCC1–AQP-1 信号通路，减少脑脊液过度分泌。

3. 综合评估体系：

- 结合 MRI、行为学测试（开放场地、水迷宫）、免疫荧光、Western blot、ELISA、流式细胞术等多种方法，全面评估治疗效果与机制。

三、对学科的启示

1. 干细胞治疗的新方向：

- 研究表明，基因增强型干细胞联合小分子药物可显著提升干细胞在恶劣微环境中的存活与功能，为神经退行性疾病、脑损伤等提供新思路。

2. 炎症与脑脊液分泌的关联机制：

- 揭示了神经免疫—脑脊液分泌轴在 PHH 发病中的作用，提示针对炎症调控可能是治疗脑积水的新靶点。

3. 从“结构修复”到“功能重建”的转变：

- 研究不仅关注脑室结构的恢复，更重视认知与运动功能的改善，体现了再生医学从解剖修复向功能重建的进步。

4. 个体化与精准治疗潜力：

- 提出超声引导移植、诱导多能干细胞（iPSCs）替代等未来方向，强调个体化治疗策略在神经再生中的应用前景。

总结：本研究通过基因工程干细胞联合药物干预，系统性地解决了 PHH 治疗中的多个瓶颈问题，不仅在动物模型中验证了其安全性与有效性，更在机制层面揭示了神经再生、免疫调节与脑脊液分泌之间的内在联系。该研究为出血后脑积水的综合治疗提供了新范式，对神经再生、干细胞治疗及神经免疫等学科具有重要的推动作用和临床转化价值。